Analytical Approach to the Torsional Behavior of Concrete Beams Reinforced with Fiber-Reinforced Polymer Bars

Cao Thanh Ngoc Tran [1,2], Vinh Sang Nguyen[3,*]

[1]School of Civil Engineering and Management, International University, Ho Chi Minh City, Vietnam

[2]Vietnam National University, Ho Chi Minh City, Vietnam

[3]Faculty of Civil Engineering, Thuyloi University, Hanoi, Vietnam

Received 06 September 2026; received in revised form 23 March 2026; accepted 26 March 2026

DOI: https://doi.org/10.46604/aiti.2026.16061

Abstract

Fiber-reinforced polymer (FRP) bars have emerged as a promising alternative to conventional steel reinforcement for improving the durability of reinforced concrete (RC) members in corrosive environments. Despite increasing experimental research, analytical models capable of capturing the pure torsional response of FRP bar-reinforced concrete beams remain scarce. This study presents a modified softened membrane model for torsion (SMMT) for solid FRP-RC beams. The proposed formulation incorporates an FRP-compatible strain-coupling relationship through a modified Hsu/Zhu approach to account for poisson’s effect. The model is validated against sixteen rectangular FRP-RC beam tests reported in the literature. Predicted cracking torque, ultimate torque, torque-twist response, and selected stirrup strain responses show good agreement with experimental results. A parametric study is further conducted to quantify the influences of concrete strength, FRP elastic modulus, and longitudinal and transverse FRP reinforcement ratios. The proposed model provides a reliable analytical framework for evaluating the torsional behavior of FRP-RC beams.

Keywords: torsion behavior, beam, FRP bars, modified softened membrane model for torsion.

1. Introduction

The long-term durability of reinforced concrete (RC) structures remains a major concern in civil, industrial, and transportation infrastructure. This issue is particularly critical in aggressive environments where corrosion of steel reinforcement accelerates deterioration and shortens service life. In this context, fiber-reinforced polymer (FRP) bars have emerged as a promising alternative to conventional steel reinforcement because of their corrosion resistance, high strength-to-weight ratio, and potential to reduce maintenance and life-cycle costs [1]. Although the flexural and shear performance of FRP bar-reinforced concrete members has been widely investigated [2-4], the torsional behavior of FRP-RC beams has received comparatively less attention. Consequently, reliable tools for predicting their full torsional response are still limited.

Torsion may govern the behavior of structural members subjected to eccentric loading, curved geometries, edge or spandrel configurations, and complex load paths. The torsional response typically progresses from a linear-elastic pre-cracking stage to a post-cracking stage characterized by marked stiffness reduction and internal force redistribution. It then transitions to a nonlinear stage approaching peak torque and post-peak softening. In FRP-RC beams, this behavior is further affected by the elastic-brittle nature of FRP reinforcement and by known limitations of FRP stirrups, such as reduced strength in bent regions and possible bond deficiencies at corners, thereby influencing both strength and deformation capacity [2].

---

* Corresponding author. E-mail address: sangnv@tlu.edu.vn

Early experimental studies clarified the torsional behavior and failure modes of FRP-RC beams and demonstrated the sensitivity of the response to stirrup detailing. These studies also highlighted the limited accuracy of existing design provisions in predicting quantities such as stirrup strain and strut inclination [5-7]. Experimental studies on beams reinforced with carbon fiber reinforced polymer (CFRP) bars as both longitudinal and transverse reinforcement reported torsional strength and crack patterns comparable to those observed in steel-RC members. However, noticeable differences were observed in the deformation characteristics and post-peak response [8]. More recently, Lei et al. [9] conducted a systematic study on BFRP-RC beams under pure torsion and demonstrated a pronounced size effect; they showed that increasing the stirrup ratio enhances both torsional strength and deformation capacity. Collectively, these studies indicate that the torsional response of FRP-RC beams is governed by the interaction among concrete cracking and softening, transverse reinforcement contribution, and the controlling failure mechanism.

Unlike conventional steel reinforcement, FRP bars show a predominantly linear-elastic response up to rupture, in contrast to the ductile behavior of steel. Consequently, major design guidelines for FRP-RC members, including ACI 440.1 R-06 [2], JSCE [3], and CSA [4], provide limited provisions for torsional resistance. JSCE [3] explicitly states that torsional design of FRP-reinforced members should be supported by reliable experimental evidence and analytical models. In addition, FRP stirrups often exhibit reduced tensile capacity compared with straight FRP bars because of strength reduction in bent regions, which can affect torsional performance and failure mode [2]. For RC members, torsional design in CSA and ACI is generally based on the thin-walled tube analogy combined with simplified space-truss concepts [10, 11]. Meanwhile, the torsion clauses in CSA S806-12 [12] are largely adapted from these established RC codes [10, 11] because of the scarcity of FRP-specific torsion data.

From a modeling perspective, torsion theories for RC members have largely evolved from truss- and membrane-based approaches originally developed for shear. A representative model is the Rotating-angle softened truss model (RA-STM), originally introduced by Rausch [13] and later refined by Vecchio and Collins [14]. Bernardo [15] further refined this model for torsion analysis of RC beams by primarily considering the compressive behavior of concrete. Although effective in representing concrete compression, the RA-STM neglects the tensile contribution of concrete. Another important framework is the compression field theory (CFT) proposed by Collins [16] and its extension, the modified compression field theory (MCFT), developed by Vecchio and Collins [14]. Rahal and Collins [17] adapted the MCFT to RC and prestressed RC beams subjected to combined shear, torsion, and bending.

The softened truss model (STM), developed by Hsu and Mo [18], incorporates concrete softening in compression for torsional analysis of RC beams. Chalioris [19] combined the smeared crack model [20] for the elastic stage with the STM for the post-cracking response. The softened membrane model (SMM) was originally proposed by Hsu and Zhu [20] and later extended by Jeng [21] for torsional analysis, resulting in the softened membrane model for torsion (SMMT). The SMMT incorporates the Hsu/Zhu ratio to represent poisson's effect under uniaxial and biaxial compression [22] and accounts for the reduction in strut strain caused by out-of-plane bending under torsion. The model has shown good agreement with experimental results and has been further developed for practical torsional analysis and design. Nevertheless, its direct application to FRP-RC beams remains limited because FRP reinforcement exhibits a linear-elastic brittle response up to rupture, unlike the yielding behavior of steel. This difference indicates the need for an FRP-consistent analytical treatment, particularly in the representation of strain coupling associated with poisson's effect.

Accordingly, the main objective of this study is to develop a practical, design-oriented analytical model for predicting the pure torsional response of solid FRP bar-reinforced concrete beams. To achieve this objective, the SMMT is modified by incorporating an FRP-compatible strain-coupling relationship through a revised Hsu/Zhu approach. The proposed model is validated using published experimental results in terms of cracking torque, ultimate torque, torque-twist response, and FRP stirrup strain response. In addition, a parametric study is conducted to examine the effects of concrete strength, FRP elastic modulus, and longitudinal and transverse reinforcement ratios.

The rest of this paper is organized as follows: Section 2 presents the analytical approaches and the formulation of the modified SMMT; Section 3 verifies the proposed model against experimental results and discusses the main findings, including the parametric study; finally, Section 4 summarizes the main conclusions.

2. Analytical Approaches

This section briefly reviews the principal analytical approaches used to describe the torsional behavior of reinforced concrete members and examines their relevance to FRP bar-reinforced concrete beams. Particular attention is given to truss- and membrane-based formulations that provide the theoretical basis for pure torsion analysis. Based on this discussion, the rationale for adopting and modifying the SMMT in the present study is introduced.

2.1 Background

Computational models for torsional behavior and strength have largely evolved from theories originally developed for shear in RC members. Representative approaches for the analysis of pure torsion include the MCFT [14], RA-STM [15], and SMMT [21, 23]. The MCFT is primarily intended for shear or combined bending-shear actions rather than pure torsion. By contrast, the RA-STM and SMMT were developed specifically to describe the pure torsional response of conventional RC members. However, their direct application to FRP-RC beams remains limited because FRP reinforcement exhibits brittle failure, unlike the ductile response of steel.

2.2 Modified SMMT for FRP bar-reinforced concrete members under torsion

This section presents the modified SMMT for FRP bar-reinforced concrete members under pure torsion. The formulation preserves the original equilibrium and compatibility framework while incorporating an FRP-compatible strain-coupling treatment associated with poisson’s effect. The governing equations and the modified Hsu/Zhu relationship are introduced in the following subsections.

2.2.1 Equilibrium equations, conditions for convergence, and compatibility equations

Fig. 1 depicts an FRP-reinforced rectangular concrete beam subjected to applied pure torque (*T*). Subject to external torque *T*, the beam structure generates an internal force resulting from a uniformly distributed shear stress flow (τ_{lt}), creating a shear flow (*q*) within the effective thickness (*td*) [24]. The equilibrium across the entire cross-sectional area is expressed by the following relationship:

$$T = \tau_{lt}\left(2A_0 t_d\right) \tag{1}$$

For a rectangular cross-section characterized by height (*h*) and width (*b*), the area and perimeter associated with the shear flow are defined as [24]:

$$A_0 = A_c - \frac{1}{2} p_c t_d + t_d^2 \tag{2}$$

$$p_0 = p_c - 4t_d \tag{3}$$

When the tensile stress of concrete reaches (*fcr*), cracks begin to form and propagate as spiral paths along the beam's axis. This results in the formation of a spatial truss mechanism consisting of inclined concrete compression struts and tension ties formed by FRP bars in the vertical and longitudinal directions of the beam. According to Saint Venant's theory, considering the stress state of a unit element *A* under pure torsion, the normal stress components in the vertical and longitudinal directions are neglected, i.e., $\sigma_l = \sigma_t = 0$ (Fig. 1 (a)-(b)). Based on the SMMT, the inclination angle of the concrete cracks, formed between axis *2* and axis *l*, is 45° [21]. Simultaneously, based on the Navier principle, the equilibrium of element *A* is ensured for tensile, compressive, and shear stresses by the following equations [24]:

$$\sigma_2^c \cos^2 \alpha_2 + \sigma_1^c \sin^2 \alpha_2 + 2\tau_{21}^c \sin\alpha_2 \cos\alpha_2 + \rho_{fl} f_{fl} = 0 \tag{4}$$

$$\sigma_2^c \sin^2 \alpha_2 + \sigma_1^c \cos^2 \alpha_2 - 2\tau_{21}^c \sin\alpha_2 \cos\alpha_2 + \rho_{ft} f_{ft} = 0 \tag{5}$$

$$\tau_{lt} = \left(\sigma_2^c + \sigma_1^c\right)\sin^2 \alpha_2 - 2\tau_{21}^c \sin\alpha_2 \cos\alpha_2 + \rho_{ft} f_{ft} \tag{6}$$

The conditions for convergence are established by integrating the in-plane equilibrium equations and are applied consistently during the computational process to ensure the precision of theoretical predictions. These conditions must be met at every step of the loading computation in the modeling process, as adopted in the SMMT [21] implementation, and are expressed as follows:

$$\rho_{fl} f_{fl} + \rho_{ft} f_{ft} = -\left(\sigma_2^c + \sigma_1^c\right) \tag{7}$$

$$\rho_{fl} f_{fl} - \rho_{ft} f_{ft} = -\left(-\sigma_2^c + \sigma_1^c\right)\cos 2\alpha_2 - 2\tau_{21}^c \sin 2\alpha_2 \tag{8}$$

Similarly, FRP-RC beams are required to satisfy local equilibrium conditions, encompassing both in-plane equilibrium within the cross-sectional plane and global equilibrium across the entire cross-sectional area of the beam. These conditions ensure that internal forces and stresses are balanced under the applied loading, maintaining structural integrity. In a structural member subjected to torsional loading, the angle of twist per unit length, denoted as (θ), induces bending deformations in the concrete struts that form part of the spatial truss mechanism resisting the torsion. This bending effect is quantified through a relationship that incorporates the average shear strain (γ_{lt}), which reflects the shear deformation resulting from the torsional moment.

Additionally, the calculation accounts for the geometric properties of the shear flow path, specifically the perimeter (p_0) and the enclosed area (A_0) of the centerline of the shear flow [25]. These parameters collectively enable a precise determination of the torsional response, ensuring that the interplay between material properties and geometric configurations is accurately captured in the analysis, as defined by the following relationship:

$$\theta = p_0 \gamma_{lt} / (2A_0) \tag{9}$$

Fig. 2(a) shows that the strain state of shear element *A* can be represented using Mohr's strain circle. This leads to the derivation of three compatibility equations, which ensure the strain components align with the element's deformation under torsion, expressed as follows:

$$\varepsilon_l = \varepsilon_2 \cos^2 \alpha_2 + \varepsilon_1 \sin^2 \alpha_2 + \gamma_{21} \sin\alpha_2 \cos\alpha_2 \tag{10}$$

$$\varepsilon_t = \varepsilon_2 \sin^2 \alpha + \varepsilon_1 \cos^2 \alpha_2 - \gamma_{21} \sin\alpha_2 \cos\alpha_2 \tag{11}$$

$$\gamma_{lt} = 2\left(-\varepsilon_2 + \varepsilon_1\right)\sin\alpha_2 \cos\alpha_2 + \gamma_{21}\left(\cos\alpha_2 - \sin\alpha_2\right) \tag{12}$$

2.2.2 *Out-of-plane bending due to torsion*

In addition to the aforementioned aspects, the distortion experienced by the thin-walled component instigates out-of-plane bending in the concrete struts oriented along the principal directions 1 and 2 (Fig. 2(b)). Specifically, the degree of curvature exhibited by these concrete struts, in direction 1, denoted as (ψ), and in direction 2, denoted as (φ), is intrinsically linked to the magnitude of the torsional twist angle (θ). This formulation highlights how torsional loading amplifies bending effects, thereby influencing the structural response. This relationship is captured by the following formulation:

$$\psi = -\varphi = \theta \sin 2\alpha_2 \tag{13}$$

Based on the core principle of linear strain distribution, commonly known as the plane-sections-remain-plane assumption in beam theory [24], the curvature parameters (ψ) and (φ) exhibit direct proportionality to essential geometric and kinematic factors. Specifically, these parameters are linked to the effective shear flow thickness (t_d), along with the mean values of tensile and compressive strains in the concrete struts. In direction 1, this encompasses the average strain ($\overline{\varepsilon_1}$), whereas in direction 2, it relates to average strain ($\overline{\varepsilon_2}$). The precise kinematic relationships governing these curvatures are expressed as follows:

$$\varphi = \bar{\varepsilon}_{1s} / t_d = 2\bar{\varepsilon}_1 / t_d \tag{14}$$

$$\psi = \bar{\varepsilon}_{2s} / t_d = 2\bar{\varepsilon}_2 / t_d \tag{15}$$

Such equations form a basis for evaluating the influence of out-of-plane effects on in-plane responses, thereby offering a more thorough depiction of strut mechanics during torsional loading. Subsequently, the average stress modification factors serve as essential multipliers in evaluating the effective average tensile stresses (k_{1t}) and compressive stresses (k_{1c}) distributed across the thickness (t_d) (Fig. 2(b)). This calculation is performed within the context of nonlinear constitutive laws governing the stress-strain behavior of concrete, accounting for material softening and cracking progression under sustained loading [24]. The average stress modification factors are defined as follows:

$$k_{1c} = \frac{1}{\zeta f_c' \bar{\varepsilon}_{2s}} \int_0^{\bar{\varepsilon}_{2s}} \sigma_2\left(\bar{\varepsilon}, \zeta\right) d\bar{\varepsilon} \tag{16a}$$

$$k_{1t} = \frac{1}{\bar{\varepsilon}_{1s} f_{cr}} \int_0^{\bar{\varepsilon}_{1s}} \sigma_1\left(\bar{\varepsilon}\right) d\bar{\varepsilon} \tag{16b}$$

To conclude this analytical process, the effective thickness (t_d) is obtained by systematically combining the governing equations. Specifically, Eqs. (2) and (3) define the geometric terms, and Eqs. (9)-(11) establish the compatibility and strain relationships. This leads to the following expressions, which deliver a closed-form solution for (t_d) and facilitate iterative numerical simulations for torsional analysis of RC members [21].

$$t_d = \frac{1}{2\times(Q+4)} \times \left[p_c \times \left(1+\frac{Q}{2}\right) - \sqrt{\left(1+\frac{Q}{2}\right)^2 \times (p_c)^2 - 4Q\times(Q+4)\times A_c} \right] \tag{17}$$

$$Q = \frac{2\bar{\varepsilon}_{2s}}{\gamma_{lt} \sin 2\alpha_2} = \frac{4\bar{\varepsilon}_2}{\gamma_{lt} \sin 2\alpha_2} \tag{18}$$

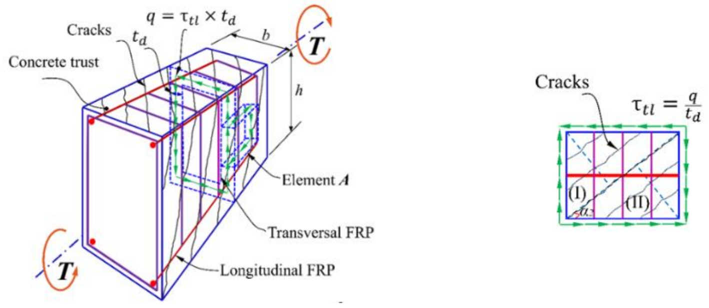

(a) FRP-reinforced concrete beam (b) Element

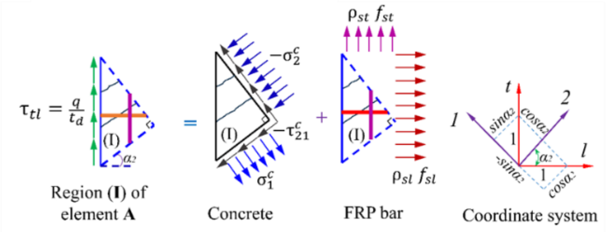

(c) Stress state of the wedge element and coordinate system

Fig. 1 FRP-reinforced rectangular concrete beam under pure torsion and plane stress state of shear element A

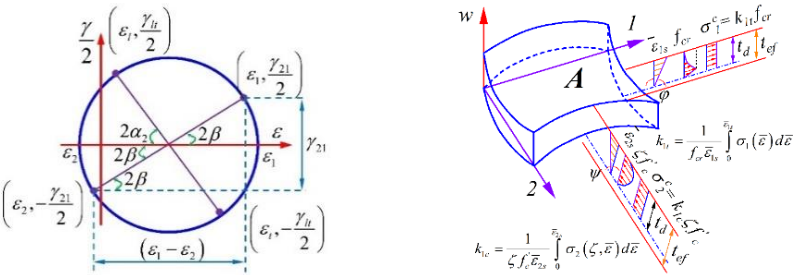

(a) Mohr's strain circle (b) Strains and stresses in concrete strut

Fig. 2 Compatibility conditions and concrete strut [24]

2.2.3 *Modified Hsu/Zhu for FRP bar in concrete member*

The strain transformation process incorporates the Hsu/Zhu amplification factors specifically tailored for torsional loading scenarios, denoted as ($(v_{12})_{torsion}$) [21]. These factors are calibrated to be approximately 0.80 times the corresponding values observed in pure shear RC members, represented as ($(v_{12})_{shear}$) [22] (Fig. 3). In previous studies, the Hsu/Zhu ratio was divided into two phases based on the yielding of steel bars. The phase prior to yielding represents the linear elastic behavior, where the constant value was 1.9 for pure shear and 1.52 for pure torsion (indicating a 20% reduction compared to the shear value). However, since FRP bars function only in the elastic range, this ratio is modified to suit the elastic phase—consistent with the behavior of standard steel in its elastic state—until the FRP bars fail, as expressed by the following relationships:

$$(\upsilon_{12})_{shear} = \begin{cases} 0.2 + 850\varepsilon_{sf} & for \ \ \varepsilon_{sf} \le \varepsilon_{fy} \\ 1.9 & for \ \ \varepsilon_{sf} > \varepsilon_{fy} \end{cases} \tag{19}$$

$$(\upsilon_{12})_{torsion} = 0.8(\upsilon_{12})_{shear} \tag{20}$$

$$(\upsilon_{12})_{torsion\_FRP} = \left(0.16 + 680\varepsilon_{sf}\right)\frac{E_{FRP}}{E_s} \quad for \ \ \varepsilon_{sf} \le \varepsilon_{fe} \tag{21}$$

Hence, the connection between uniaxial and biaxial strains caused by the poisson effect, as determined through the Hsu/Zhu ratio, for FRP-RC members under pure torsion is illustrated as follows:

$$\bar{\varepsilon}_1 = \varepsilon_1 + \left(\upsilon_{12}\right)_{torsion\_FRP} \varepsilon_2 \text{ ; and } \bar{\varepsilon}_2 = \varepsilon_2 \tag{22}$$

Substituting Eq. (22) into Eqs. (10) and (11), the calculation involves determining the strains in the longitudinal direction ($\bar{\varepsilon}_l$) and the vertical direction ($\bar{\varepsilon}_t$), achieved through the application of the following expressions as outlined in the referenced work [21]:

$$\bar{\varepsilon}_l = \bar{\varepsilon}_2 \cos^2 \alpha_2 + \bar{\varepsilon}_1 \sin^2 \alpha_2 + \gamma_{12} \sin \alpha_2 \cos \alpha_2 \tag{23}$$

$$\bar{\varepsilon}_t = \bar{\varepsilon}_2 \sin^2 \alpha_2 + \bar{\varepsilon}_1 \cos^2 \alpha_2 - \gamma_{12} \sin \alpha_2 \cos \alpha_2 \tag{24}$$

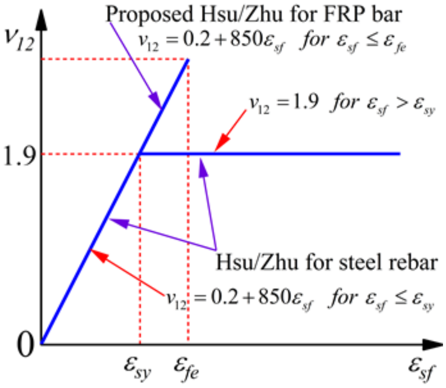

Fig. 3 Modified Hsu/Zhu for FRP bar

2.3 *Constitutive laws for FRP reinforcement and concrete*

This section summarizes the constitutive laws adopted in the modified SMMT for FRP reinforcement and concrete. The model considers the linear-elastic behavior of FRP bars up to rupture, together with the compressive softening and tensile response of concrete. These relationships form the material basis for predicting the torsional response of FRP-RC members.

2.3.1 *Stress-strain relationship for FRP reinforcement*

The uniaxial stress–strain relationship of FRP reinforcement (longitudinal bars and stirrups) is assumed to be linearly elastic up to rupture. The corresponding stress–strain curve is shown in Fig. 4(a). According to ACI 440.1R-15 [26], the allowable design stress in FRP bars is defined as follows:

$$f_f = E_f \varepsilon_f \le f_{fb} \tag{25}$$

where ffb indicates the strength of the bent region in the FRP bars. This provision is designed to regulate the extent of shear crack openings and to preclude damage to the curved segments of the FRP transverse reinforcements.

2.3.2 *Stress-strain relationship for concrete in compressive*

Within the SMMT, the stress-strain relationship for concrete under compression accounts for the softening effect, as shown in Fig. 4(b). The softening coefficient (ζ) plays an important role in the model because it increases the effective wall thickness and decreases the lever arm area, thereby reducing the overestimation of torsional capacity observed in earlier models.

Following Hsu et al. [20, 24], this coefficient is defined as a function of the principal tensile strain ($\bar{\varepsilon}_1$), the concrete compressive strength (f_c'), and the deviation angle (f_c'). The average compressive stress (σ_2^c) is calculated by multiplying the average stress factor (k_{1c}), the softening coefficient (ζ), and the concrete compressive strength (f_c'), as follows:

$$k_{1c} = \left[\frac{\bar{\varepsilon}_{2s}}{\varepsilon_p} - \frac{1}{3}\left(\frac{\bar{\varepsilon}_{2s}}{\varepsilon_p} \right)^2 \right] \quad for \quad \frac{\bar{\varepsilon}_{2s}}{\varepsilon_p} \leq 1 \tag{26}$$

$$k_{1c} = 1 - \frac{1}{3}\frac{\varepsilon_p}{\bar{\varepsilon}_{2s}} - \frac{\left(\bar{\varepsilon}_{2s} - \varepsilon_p\right)^3}{3\bar{\varepsilon}_{2s}\left(4\varepsilon_0 - \varepsilon_p\right)^2} \quad for \quad \frac{\bar{\varepsilon}_{2s}}{\varepsilon_p} > 1 \tag{27}$$

$$\zeta = \frac{5.8}{\sqrt{f_c'}} \frac{1}{\sqrt{1 + 400\bar{\varepsilon}_1}} \left(1 - \frac{|\beta|}{24^0}\right) \leq 0.9 \quad and \quad \frac{5.8}{\sqrt{f_c'}} \leq 0.9 \tag{28}$$

$$\beta(\deg) = \frac{1}{2}\tan^{-1}\left(\frac{\gamma_{21}}{\varepsilon_2 - \varepsilon_1}\right)\frac{180}{\pi} \tag{29}$$

$$\sigma_2^c = -k_{1c}\zeta f_c' \tag{30}$$

2.3.3 *Stress-strain relationship for concrete in tension*

Moreover, the SMMT accounts for the tensile stress of concrete in its equations, enabling precise modeling of the early elastic portion of the torque-twist curve before cracking begins. This capability enhances the model's applicability to the full range of torsional behavior. The constitutive law governing the tensile response of concrete is graphically represented in Fig. 4(c). The evaluation of the mean tensile stress (σ_1^c) and the associated mean stress factor (k_{1t}) is mathematically defined through expressions that integrate factors like strain gradients and material properties to yield averaged values suitable for shear analysis [21]. These relationships are expressed as follows:

$$k_{1t} = \frac{\bar{\varepsilon}_{1s}}{2\varepsilon_{cr}} \quad for \quad \frac{\bar{\varepsilon}_{1s}}{\varepsilon_{cr}} \leq 1 \tag{31}$$

$$k_{1t} = \frac{\bar{\varepsilon}_{1s}}{2\varepsilon_{cr}} + \frac{\left(\varepsilon_{cr}\right)^{0.4}}{\left(1 - C\right)\bar{\varepsilon}_{1s}}\left[\left(\bar{\varepsilon}_{1s}\right)^{0.6} - \left(\varepsilon_{cr}\right)^{0.6}\right] \quad for \quad \frac{\bar{\varepsilon}_{1s}}{\varepsilon_{cr}} > 1 \tag{32}$$

$$\varepsilon_{cr} = 0.000116 \quad and \quad f_{cr} = 0.652\sqrt{f_c'} \tag{33}$$

$$\sigma_1^c = k_{1t} f_{cr} \tag{34}$$

In addition, the shear stress in the principal *1-2* coordinate system (τ_{21}^c) is quantified through the interplay between the computed average tensile and compressive stresses. This relationship ensures equilibrium in the shear flow and aligns with the overall torsional mechanics of the element [21]. The precise mathematical expression for this component is expressed as follows:

$$\tau_{21}^c = \frac{\sigma_1^c - \sigma_2^c}{2\left(\varepsilon_1 - \varepsilon_2\right)}\gamma_{21} \tag{35}$$

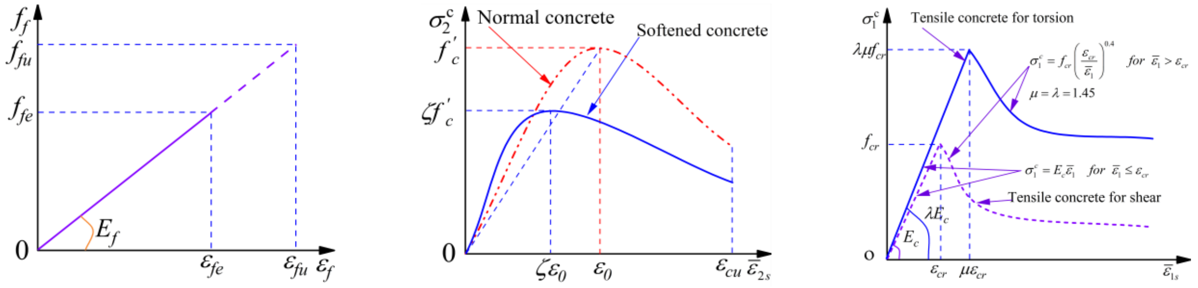

(a) FRP bar (b) Compressive in concrete (c) Tensile in concrete

Fig. 4 Constitutive stress-strain laws of FRP bar and concrete

2.4 Solution algorithm

Fig. 5 presents the computational flowchart of the modified SMMT. A MATLAB-based numerical algorithm [27] was developed to predict the torque-twist response by integrating the revised equilibrium, compatibility, and constitutive relationships. The analysis begins with the input of material properties, section geometry, and reinforcement details. An iterative procedure is then performed by increasing ε_2 from zero in increments of 0.0001 and solving for γ_{21} and ε_1 at each step to generate the theoretical torque-twist curve. The computation is terminated when the principal concrete compressive strain, ε_2, reaches -0.0035.

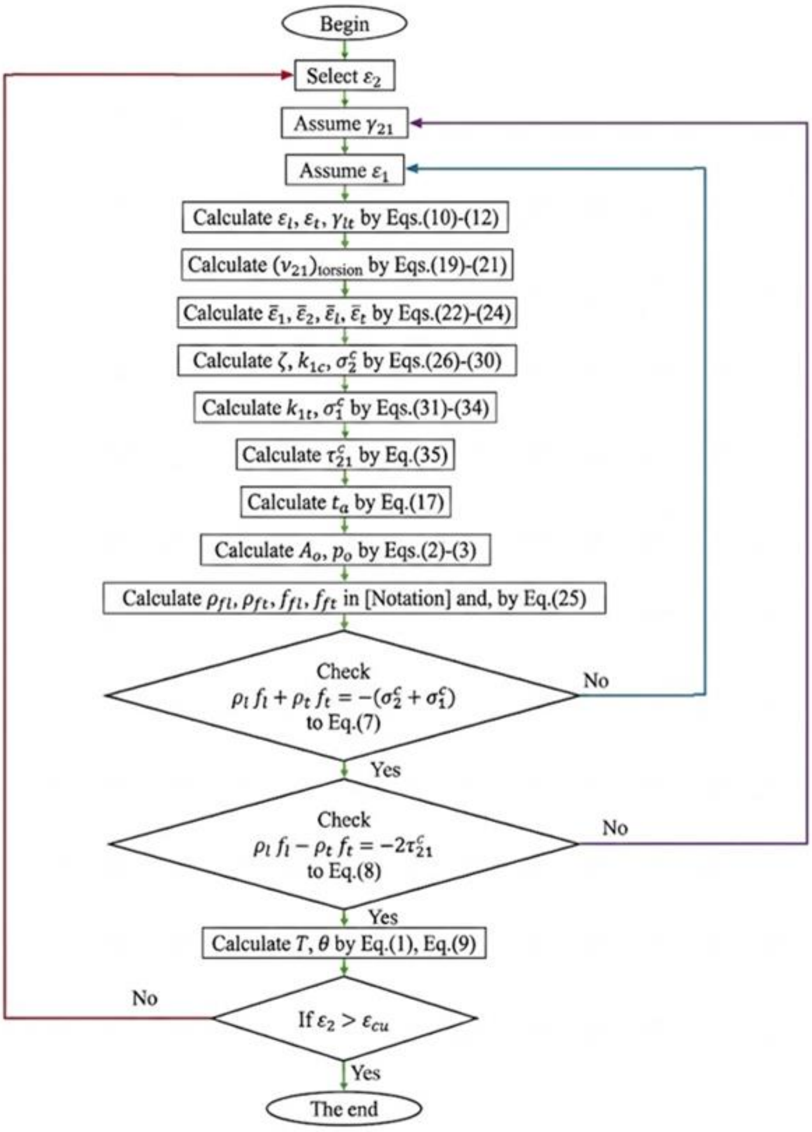

Fig. 5 The solution process for the modified SMMT

3. Verification and Discussion

This section verifies the proposed modified SMMT against published test results for FRP-RC beams under pure torsion. The model performance is assessed using torque-twist response, torsional strength, and representative FRP stirrup strains, followed by a parametric study on the effects of key material and reinforcement parameters.

3.1 Database

In recent years, multiple studies have been undertaken to analyze the torsional performance of FRP-RC beams [8, 9, 28]. The reliability of the proposed model is evaluated through a comparison between experimental results and model predictions. Details of the materials and reinforcement types used in all beams are summarized in Table 1.

Table 1 Summary of experimental data obtained from existing literature

Ref.	Beams	Section	f_c' (MPa)	Bar type	Longitudinal bars			Stirrups			
		$b\times h$ (mm)			A_{sl} (mm^2)	E_{fl} (GPa)	f_{fu} (MPa)	A_{st} (mm^2)	s (mm)	E_{ft} (GPa)	f_{fu} (MPa)
Lei et al. [9]	S-0.3-T	100×300	41.3	BFRP	678.6	49.3	1099.2	50.3	360	52.5	1157.6
	S-0.6-T	100×300	41.3	BFRP	678.6	49.3	1099.2	50.3	240	52.5	1157.6
	S-0.9-T	100×300	41.3	BFRP	678.6	49.3	1099.2	50.3	120	52.5	1157.6
	M-0.3-T	200×600	41.3	BFRP	2871.4	44.8	1018.5	50.3	360	52.5	1157.6
	M-0.6-T	200×600	41.3	BFRP	2871.4	44.8	1018.5	50.3	240	52.5	1157.6
	M-0.9-T	200×600	41.3	BFRP	2871.4	44.8	1018.5	50.3	120	52.5	1157.6
	L-0.3-T	300×900	41.3	BFRP	6421.4	44.1	824.7	50.3	360	52.5	1157.6
	L-0.6-T	300×900	41.3	BFRP	6421.4	44.1	824.7	50.3	240	52.5	1157.6
	L-0.9-T	300×900	41.3	BFRP	6421.4	44.1	824.7	50.3	120	52.5	1157.6
Mohamed et al. [8]	BC120	250×600	38.5	CFRP	1013.4	144	1765	71.0	120	130	1562
	BC180	250×600	38.5	CFRP	1013.4	144	1765	71.0	180	130	1562
	BC240	250×600	38.5	CFRP	1013.4	144	1765	71.0	240	130	1562
	BC300	250×600	38.5	CFRP	1013.4	144	1765	71.0	300	130	1562
Mohamed et al.[28]	BC60	250×600	39.25	CFRP	1013.4	144	1765	71.0	60	130	1562
	BG60	250×600	39.25	GFRP	1984.7	64.7	948	71.0	60	44.8	948
	BG120	250×600	39.25	GFRP	1984.7	64.7	948	71.0	120	44.8	948

3.2 Torsional behavior

Fig. 6 compares the experimental torque-angle of twist response curve of specimen L-0.9-T [9] with predictions from the unmodified SMMT and the proposed modified SMMT. Both models reproduce the overall trend of torsional hardening toward peak torque; however, the unmodified SMMT predicts higher cracking and ultimate torques than the modified formulation. This difference is attributed to the poisson-effect-related strain-coupling (Hsu/Zhu) treatment, which is the only component changed between the two analyses and directly affects the evolution of principal tensile strain and post-cracking force redistribution. The modified SMMT yields a response closer to the experimental peak trend for this specimen, indicating that the FRP-oriented calibration of the Hsu/Zhu coupling improves torsional prediction in both the pre-cracking and post-cracking phases.

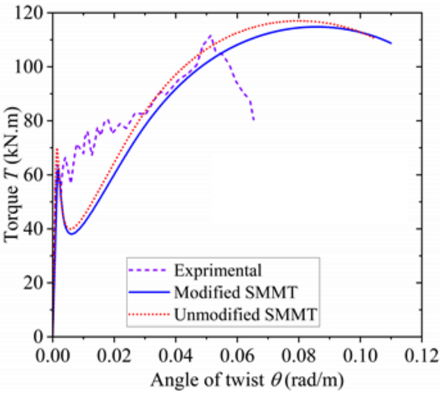

Fig. 6 Experimental and predicted torque-angle of twist responses of L-0.9-T using unmodified and modified SMMT [9]

Fig. 7 provides a comparison between the predicted torque-twist curves obtained from the modified SMMT and the corresponding experimental results. To break this down, Fig. 7(a)–(f) illustrates the FRP-RC beams tested by Lei et al. [9], demonstrating the model's capability to capture the torsional response across different configurations. Fig. 7(g)–(i) corresponds to the specimens tested by Mohamed et al. [8], emphasizing differences in reinforcement ratios and material properties. Fig. 7(k)–(m) corresponds to the beams tested by Mohamed and Benmokrane [28], which include additional variables such as beam dimensions and loading conditions.

Overall, the theoretical predictions from the modified SMMT demonstrate excellent congruence with the experimental torque-twist curves. The model effectively reproduces key performance metrics like ultimate torsional strength, the initial linear elastic phase prior to cracking, and the nonlinear post-elastic stiffening leading up to the peak torque. This alignment underscores the model's robustness in capturing the progressive damage mechanisms, such as crack initiation and propagation, under torsional loading.

Nevertheless, a discrepancy was observed in the post-peak regime. The experimental curves exhibit a steeper degradation in load-carrying capacity compared to the model's forecasts, indicating a more abrupt failure behavior in the experiments. This observed discrepancy logically stems from the SMMT's explicit integration of the Poisson effect, which influences strain transformations and softening behaviors. As a result, the model may overestimate residual stiffness post-peak, as was corroborated by similar observations in prior studies [29]. Such insights not only validate the model's pre-peak fidelity but also highlight opportunities for further refinement to enhance post-peak accuracy, potentially through incorporating additional factors like localized buckling or fiber debonding in FRP reinforcements.

3.3 Torsional strength

Table 2 summarizes the experimental and analytical values for cracking torsional moment (T_{cr}) and ultimate torsional moment (T_u), along with the corresponding twist angles per unit length (θ_{cr} and θ_u) for 16 beams collected from published studies. The proposed model shows good agreement with the experimental results. For the cracking torsional strength, the mean value (MV) of the ratio ($T_{cr,cal}/T_{cr,exp}$) is 1.09, with a standard deviation (SD) of 0.08. For the ultimate torsional strength, the MV of the ratio ($T_{u,cal}/T_{u,exp}$) is 1.03, with an SD of 0.07. Meanwhile, for the ratios ($\theta_{cr,cal}/\theta_{cr,exp}$) and ($\theta_{u,cal}/\theta_{u,exp}$) the mean values are 0.67 and 2.35, and the corresponding standard deviations are 0.27 and 1.15, respectively. Overall, these results indicate that the proposed model predicts torsional strength (T_{cr} and T_u) reasonably well in both pre- and post-cracking stages, whereas accurate estimation of the angle of twist (θ_{cr} and θ_u) remains more challenging.

Compared with strength, twist is a deformation quantity accumulated from the evolving post-cracking stiffness and is therefore highly sensitive to several factors: (i) boundary conditions and warping restraint; (ii) crack localization and instability near the peak and post-peak regimes; and (iii) bond/interface degradation and bent-stirrup corner effects, which are not explicitly represented in a sectional smeared-strain SMMT framework. Strength predictions are generally more robust because they are primarily governed by global equilibrium and the limiting capacity of the reinforcement–strut mechanism. Future improvements should incorporate boundary/warping-restraint corrections and localization-aware softening, such as fracture-energy or characteristic-length concepts. Additionally, FRP–concrete interface softening or bond–slip relationships, together with refined numerical stepping around cracking, are needed to enhance θ-prediction accuracy.

Table 2 Comparison of proposed model and previous experimental results

Ref.	Beams	T_{cr} (kN.m)			θ_{cr} (rad/m)			T_u (kN.m)			θ_u (rad/m)		
		$T_{cr,exp}$	$T_{cr,cal}$	$T_{cr,cal}$ $/T_{cr,exp}$	$\theta_{cr,exp}$	$\theta_{cr,cal}$	$\theta_{cr,cal}$ $/\theta_{cr,exp}$	$T_{u,exp}$	$T_{u,cal}$	$T_{u,cal}$ $/T_{u,exp}$	$\theta_{u,exp}$	$\theta_{u,cal}$	$\theta_{u,cal}$ $/\theta_{u,exp}$
Lei et al. [9]	S-0.3-T	3.12	3.68	1.18	0.0055	0.0045	0.83	4.56	4.51	0.99	0.0962	0.2628	2.73
	S-0.6-T	3.45	3.39	0.98	0.0060	0.0053	0.89	4.25	5.29	1.24	0.1774	0.2513	1.42
	S-0.9-T	3.35	3.12	0.93	0.0060	0.0055	0.92	5.66	5.58	0.99	0.1648	0.2516	1.53
	M-0.3-T	17.60	19.98	1.14	0.0137	0.0029	0.21	27.43	27.06	0.99	0.0877	0.1445	1.65
	M-0.6-T	18.20	20.06	1.10	0.0127	0.0028	0.22	32.07	33.90	1.06	0.0794	0.1319	1.66
	M-0.9-T	20.18	20.12	1.00	0.0073	0.0028	0.39	36.71	38.46	1.05	0.0823	0.1252	1.52
	L-0.3-T	52.25	61.98	1.19	0.0042	0.0019	0.46	76.25	80.51	1.06	0.0358	0.1026	2.87
	L-0.6-T	60.22	62.19	1.03	0.0038	0.0019	0.50	103.3	101.06	0.98	0.0445	0.0916	2.06
	L-0.9-T	63.62	62.35	0.98	0.0015	0.0019	1.27	111.6	114.84	1.03	0.0514	0.0865	1.68
Mohamed et al. [8]	BC120	30.45	32.15	1.06	0.0022	0.0017	0.75	62.88	60.10	0.96	0.0447	0.0987	2.21
	BC180	29.87	32.15	1.08	0.0019	0.0017	0.88	49.40	53.41	1.08	0.0357	0.1073	3.00
	BC240	27.45	32.15	1.17	0.0021	0.0017	0.79	39.38	40.86	1.04	0.0229	0.1193	5.21
	BC300	26.78	32.15	1.20	0.0018	0.0017	0.92	35.67	38.49	1.08	0.0235	0.1199	5.10
Mohamed et al.[28]	BC60	30.14	32.15	1.07	0.0022	0.0017	0.75	69.28	66.16	0.95	0.0412	0.0952	2.31
	BG60	27.76	32.15	1.16	0.0043	0.0017	0.38	56.86	53.96	0.95	0.0748	0.1031	1.38
	BG120	27.46	32.15	1.17	0.0026	0.0017	0.63	52.65	52.00	0.99	0.0843	0.1013	1.20
Mean values (MV)				1.09	-		0.67	-		1.03	-		2.35
Standard deviation (SD)				0.08			0.27			0.07			1.15

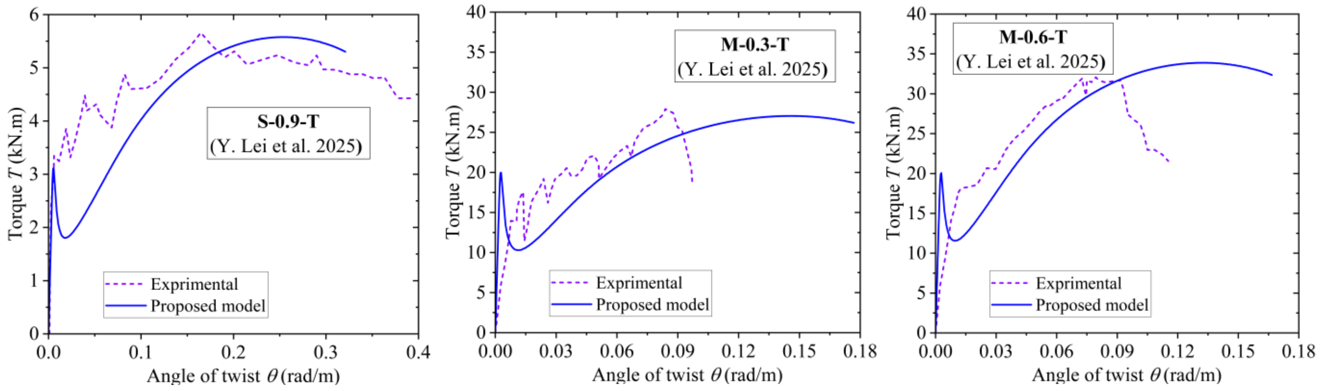

(a) S-0.9-T (b) M-0.3-T (c) M-0.6-T

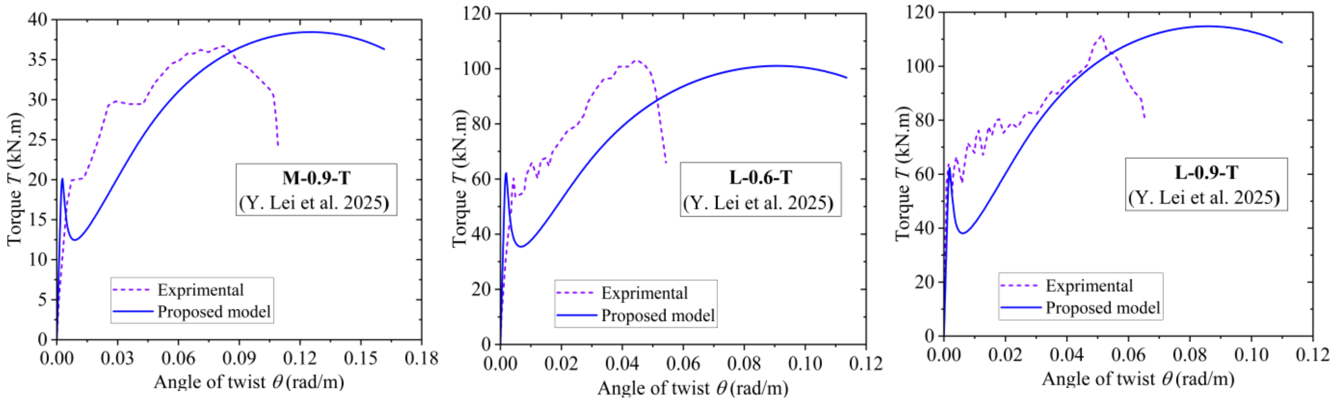

(d) M-0.9-T (e) L-0.6-T (f) L-0.9-T

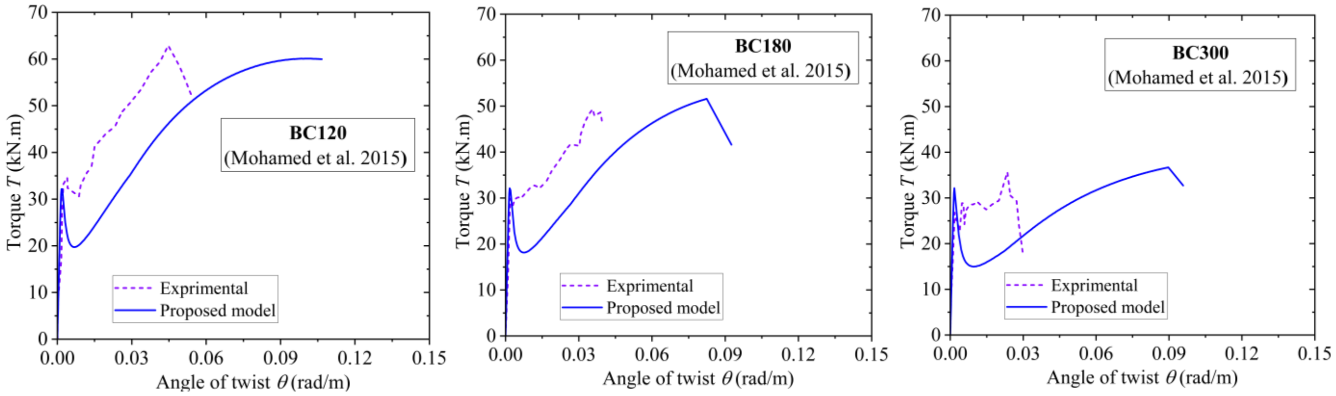

(g) BC120 (h) BC180 (i) BC300

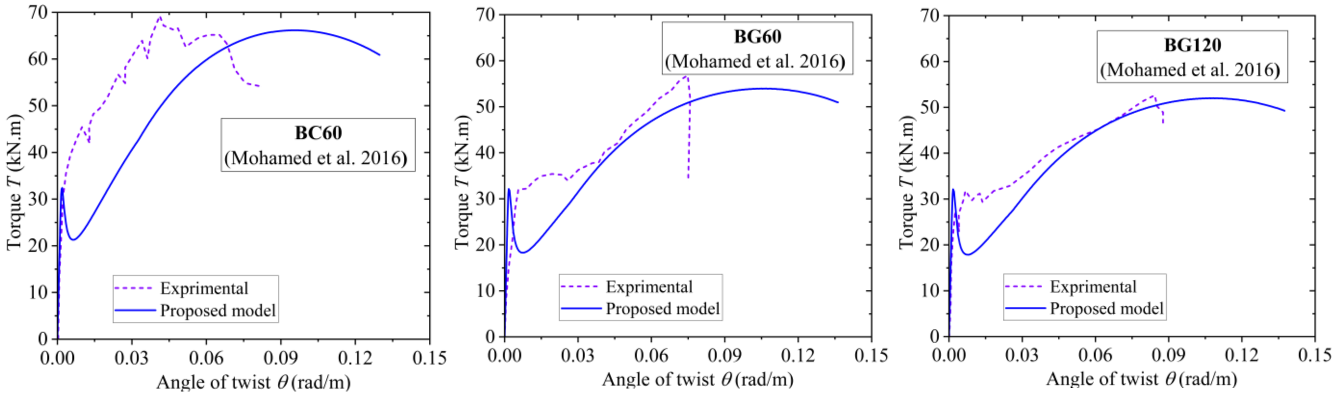

(k) BC160 (l) BG60 (m) BG120

Fig. 7 Experimental and analytical torque-angle of twist curves of beams

3.4 Torque-strain relationship curves

Fig. 8 depicts the correlation between the FRP stirrup strain and the applied torsional moment. Only six representative beams are shown because complete torque–stirrup strain histories were available only for these specimens in the collected database. In general, the results demonstrate that the proposed model captures the measured stirrup strain response with reasonable accuracy across the main torsional stages. Prior to cracking, stirrup strains remain small, implying limited participation of transverse reinforcement in the uncracked elastic regime. After crack initiation, stirrup strains increase markedly, reflecting the redistribution of torsional resistance from the cracked concrete to the transverse FRP reinforcement. With further increase in torque, the stirrup strains continue to grow; for stirrups intersecting dominant inclined cracks, the strain approaches the reported rupture strain of approximately 0.004 [26].

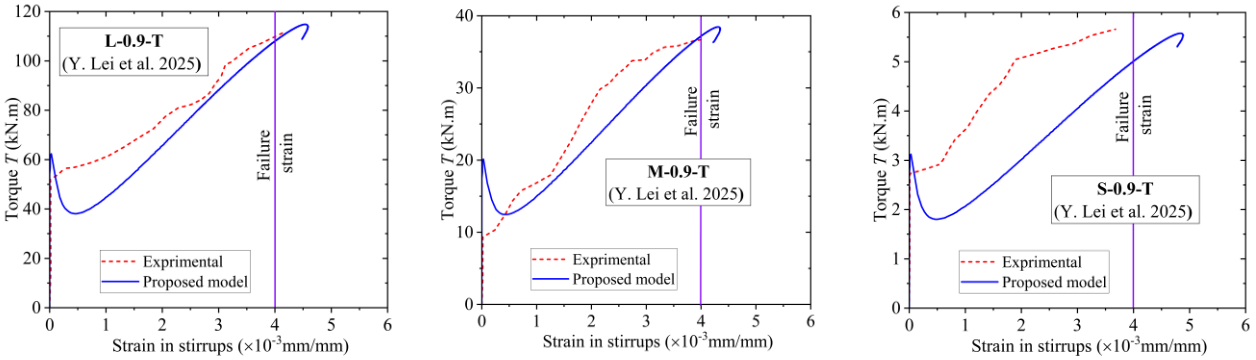

(a) L-09-T (b) M-0.9-T (c) S-0.9-T

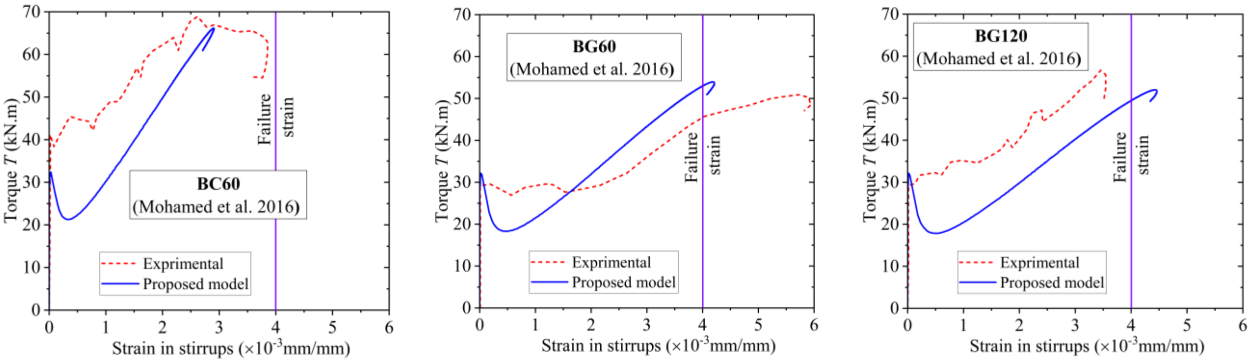

(d) BC60 (e) BG60 (f) BG120

Fig. 8 Experimental and analytical torque-strain curves

4. Parametric Study

Numerous prior experimental investigations established that factors such as size effect, compressive strength of concrete, strength of FRP material, and FRP ratio substantially influence torsional strength and response [8, 9, 28]. However, experimental research is often costly and time-consuming, whereas finite element modeling may have difficulty reproducing the boundary conditions used in experimental testing [23].

Given that the proposed model has shown satisfactory capability in reproducing the torsional response of FRP-RC beams, a parametric investigation is conducted to examine the effects of key parameters. The parametric study considers the concrete compressive strength (f_c'), the FRP elastic modulus and reinforcement ratio in the longitudinal direction (E_{fl}, ρ_{fl}), and those in the transverse direction (E_{ft}, ρ_{ft}). The specimen M-0.6-T tested by Lei et al. [9] was adopted as the baseline case.

Fig. 9 summarizes the parametric trends predicted by the proposed model for the M-0.6-T specimen tested by Lei et al. [9]. As shown in Fig. 9(a), increasing the concrete compressive strength f_c' (20–60 MPa) consistently elevates the entire T–θ

response, leading to noticeable increases in both the cracking torque T_{cr} and the ultimate torque T_u; this reflects the role of concrete in controlling crack initiation and, at higher load levels, the capacity and softening resistance of the compression strut field.

By contrast, the longitudinal FRP parameters have only a limited effect on torsional capacity. Increasing the longitudinal FRP elastic modulus Efl in Fig. 9(b) and the longitudinal FRP ratio ρfl in Fig. 9(c) causes little change in Tcr and only a modest increase in T_u. In comparison, the transverse reinforcement parameters strongly influence the post-cracking response. As shown in Fig. 9 (d), increasing the transverse FRP elastic modulus Eft significantly improves post-cracking torsional resistance and T_u, while T_{cr} remains nearly unchanged.

The greatest sensitivity is observed for the transverse FRP ratio ρ_{ft} in Fig. 9(e). Although T_{cr} remains nearly insensitive to ρ_{ft}, T_u increases substantially as ρ_{ft} increases, demonstrating the governing role of transverse reinforcement in carrying the principal tensile demand and stabilizing the cracked torsional mechanism. The strengthening benefit, however, gradually saturates at higher ρ_{ft} levels (around the higher-range cases shown), as the governing failure mode shifts toward concrete compression strut crushing/softening, beyond which additional transverse reinforcement cannot significantly increase T_u. Collectively, Fig. 9 confirms that $f_c{}'$ primarily governs cracking resistance and contributes to peak capacity, longitudinal FRP properties have a comparatively minor effect under pure torsion, and transverse FRP stiffness and ratio control the post-cracking stiffness evolution and ultimate torsional capacity.

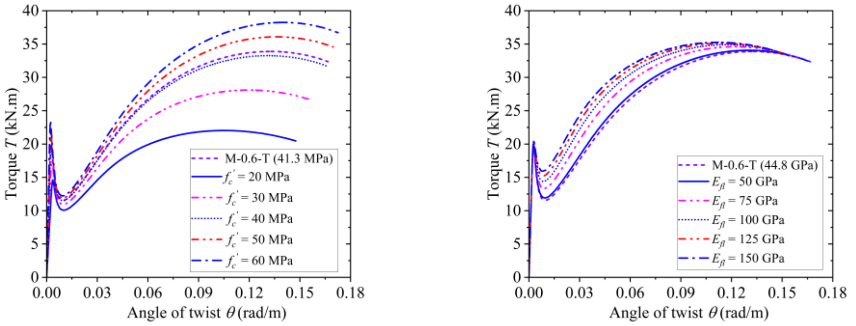

(a) Effects of $f_c{}'$ (b) Effects of E_{fl}

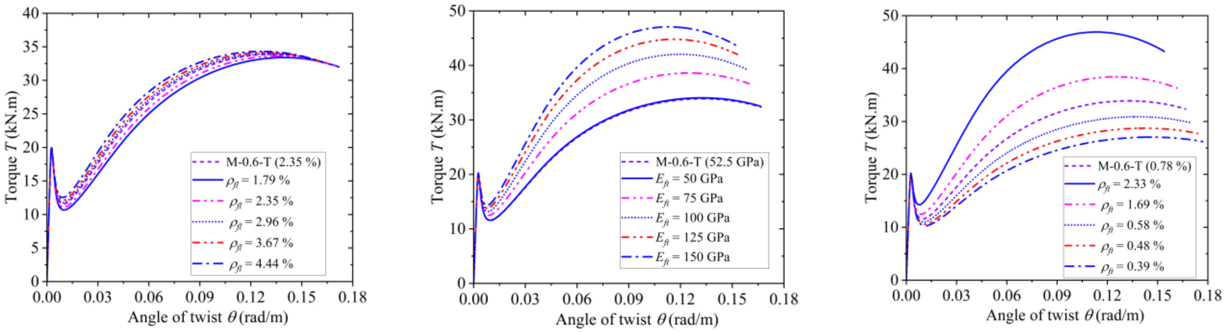

(c) Effects of ρ_{fl} (d) Effects of E_{ft} (e) Effects of ρ_{ft}

Fig. 9 Effects of concrete strength, Ef and ρf on the torsional response of specimen M-0.6-T [9]

5. Conclusion

This study developed and validated a modified SMMT to predict the pure torsional response of solid-section FRP bar–reinforced concrete beams. The proposed enhancement introduces an FRP-consistent strain-coupling treatment associated with poisson's effect, enabling a more appropriate representation of the elastic behavior of FRP reinforcement in torsion. The main conclusions are as follows:

(1) The improved SMMT reasonably predicts the complete torque-twist response, including pre-cracking and post-cracking stages, as well as ultimate torsional strength and cracking torque. The model yields mean strength ratios of $T_{cr,cal}/T_{cr,exp}$ =

1.09 (SD = 0.08) and $T_{u,cal}/T_{u,exp}$ = 1.03 (SD = 0.07), indicating good agreement for both cracking and ultimate torsional capacities.

(2) The model reproduces the overall torque–twist response satisfactorily in the pre-cracking and post-cracking regimes. However, the predicted post-peak branch is generally smoother than experiments, reflecting the smeared-strain nature of the formulation and the lack of explicit localization and interface degradation mechanisms.

(3) The proposed model captures the torque–stirrup strain trend for representative beams: stirrup strains remain small before cracking, then increase markedly after cracking as torsional resistance progressively transfers from concrete to transverse FRP reinforcement, ultimately approaching rupture strains consistent with design recommendations.

(4) The parametric investigation shows that increasing f_c' increases both T_{cr} and T_u, while transverse FRP stiffness/ratio (E_{ft}, ρ_{ft}) mainly governs post-cracking resistance and T_u. Longitudinal FRP stiffness and reinforcement ratio (E_{fl}, ρ_{fl}) have a comparatively minor influence under pure torsion. Strength gains from increasing ρ_{ft} tend to saturate at higher ρ_{ft} levels when failure becomes governed by compression-strut crushing/softening.

The proposed modified SMMT offers a practical analytical tool for evaluating torsional capacity and stiffness evolution of solid-section FRP-RC beams. It supports design-oriented assessment where current codes provide limited torsion provisions for FRP-RC members. Future work should focus on improving twist and post-peak predictions by incorporating warping-restraint/boundary corrections, localization-aware softening (fracture-energy/characteristic-length concepts), and bond–slip relationships

Acknowledgments

This research is funded by Vietnam National University Ho Chi Minh City (VNU-HCM) under a project within the framework of the Program titled “Strengthening the capacity for education and basic scientific research integrated with strategic technologies at VNU-HCM, aiming to achieve advanced standards comparable to regional and global levels during the 2025-2030 period, with a vision toward 2045.

Conflicts of Interest

The authors declare no conflict of interest.

References

[1] H. M. Mohamed and B. Benmokrane, "Design and Performance of Reinforced Concrete Water Chlorination Tank Totally Reinforced with GFRP Bars: Case Study," Journal of Composites for Construction, vol. 18, no. 1, article no. 05013001, 2014.

[2] ACI Committee 440, "Guide for the Design and Construction of Structural Concrete Reinforced with FRP Bars (ACI 440.1R-06)," Farmington Hills, MI, USA: American Concrete Institute, 2006.

[3] JSCE, "Recommendations for Upgrading of Concrete Structures with Use of Continuous Fiber Sheets," Japanese Society of Civil Engineers, Tokyo, Japan, 2001.

[4] Canadian Standards Association (CSA), "Design of Concrete Structures (CAN/CSA-A23.3-94)," Rexdale, ON, Canada, 1994.

[5] A. Deifalla, M. Hamed, A. Saleh, and T. Ali, "Exploring GFRP Bars as Reinforcement for Rectangular and L-Shaped Beams Subjected to Significant Torsion: An Experimental Study," Engineering Structures, vol. 59, pp. 776-786, 2014.

[6] V. S. Nguyen, X. H. Nguyen, D. D. Le, C. T. N. Tran, and A. D. Nguyen, "Experimental Studies on Torsional Behavior of Reinforced Concrete Beams Strengthened Using Hybrid Carbon and Basalt FRP Sheets," Structural Concrete, vol. 26, no. 5, pp. 6594-6618, 2025.

[7] I. T. Mostafa, S. Mousa, H. M. Mohamed, and B. Benmokrane, "Strength and Behavior of Glass Fiber-Reinforced Polymer-Reinforced Concrete Box Girders without Web Reinforcement under Pure Torsion," ACI Structural Journal, vol. 120, no. 5, pp. 63-76, 2023.

[8] O. Chaallal, H. M. Mohamed, and B. Benmokrane, "Torsional Moment Capacity and Failure Mode Mechanisms of Concrete Beams Reinforced with Carbon FRP Bars and Stirrups," Journal of Composites for Construction, vol. 19, no. 2, article no. 04014049, 2015.

[9] D. Li, Y. Lei, L. Jin, and X. Du, "Experimental Study on Torsional Size Effect of BFRP Bars-RC Beams," Engineering Structures, vol. 326, article no. 119595, 2025.

[10] Canadian Standards Association (CSA), "Design of Concrete Structures (CAN/CSA-A23.3-04)," Mississauga, ON, Canada, 2004.

[11] ACI Committee 318, "Building Code Requirements for Structural Concrete (ACI 318-05)," Farmington Hills, MI, USA: American Concrete Institute, 2005.

[12] Canadian Standards Association (CSA), "Design and Construction of Building Structures with Fibre-Reinforced Polymers (CAN/CSA-S806-12)," Toronto, ON, Canada, 2012.

[13] E. Rausch, Berechnung des Eisenbetons gegen Verdrehung (Torsion) und Abscheren. Berlin, Germany: Springer, 1938.

[14] F. J. Vecchio and M. P. Collins, "The Modified Compression-Field Theory for Reinforced Concrete Elements Subjected to Shear," ACI Journal Proceedings, vol. 83, no. 2, pp. 219-231, 1986.

[15] L. F. A. Bernardo and S. M. R. Lopes, "Behaviour of Concrete Beams under Torsion: NSC Plain and Hollow Beams," Materials and Structures, vol. 41, no. 6, pp. 1143-1167, 2008.

[16] D. Mitchell and M. P. Collins, "Diagonal Compression Field Theory-A Rational Model for Structural Concrete in Pure Torsion," ACI Journal Proceedings, vol. 71, no. 8, pp. 396-408, 1974.

[17] K. N. Rahal and M. P. Collins, "Combined Torsion and Bending in Reinforced and Prestressed Concrete Beams," ACI Structural Journal, vol. 100, no. 2, pp. 157-165, 2003.

[18] T. T. C. Hsu and Y. L. Mo, "Softening of Concrete in Torsional Members-Theory and Tests," ACI Journal Proceedings, vol. 82, no. 3, pp. 290-303, 1985.

[19] C. E. Chalioris, "Behaviour Model and Experimental Study for the Torsion of Reinforced Concrete Members," WIT Transactions on the Built Environment, vol. 85, pp. 459-468, 2006.

[20] T. T. C. Hsu and R. R. H. Zhu, "Softened Membrane Model for Reinforced Concrete Elements in Shear," ACI Structural Journal, vol. 99, no. 4, pp. 460-469, 2002.

[21] C. H. Jeng and T. T. C. Hsu, "A Softened Membrane Model for Torsion in Reinforced Concrete Members," Engineering Structures, vol. 31, no. 9, pp. 1944-1954, 2009.

[22] R. R. H. Zhu and T. T. C. Hsu, "Poisson Effect in Reinforced Concrete Membrane Elements," ACI Structural Journal, vol. 99, no. 5, pp. 631-640, 2002.

[23] A. D. Nguyen, V. S. Nguyen, X. H. Nguyen, D. D. Le, and C. T. N. Tran, "Softened Membrane Model for Forecasting Torsional Response of Reinforced Concrete Beams Strengthened Using FRP Sheets," Advances in Structural Engineering, vol. 28, no. 16, pp. 3019-3043, 2025.

[24] T. T. C. Hsu, Unified Theory of Reinforced Concrete. Boca Raton, FL, USA: CRC Press, 1993.

[25] T. T. C. Hsu and Y. L. Mo, Unified Theory of Concrete Structures. West Sussex, UK: John Wiley & Sons, 2010.

[26] ACI Committee 440, "Guide for the Design and Construction of Structural Concrete Reinforced with FRP Bars (ACI 440.1R-15)," Farmington Hills, MI, USA: American Concrete Institute, 2015.

[27] The MathWorks, Inc., MATLAB R2023a. Natick, MA, USA, 2023.

[28] H. M. Mohamed and B. Benmokrane, "Reinforced Concrete Beams with and without FRP Web Reinforcement under Pure Torsion," Journal of Bridge Engineering, vol. 21, no. 3, article no. 04015070, 2016.

[29] L. F. A. Bernardo, B. M. V. C. Filho, and B. Horowitz, "Efficient Softened Truss Model for Prestressed Steel Fiber Concrete Membrane Elements," Journal of Building Engineering, vol. 40, article no. 102363, 2021.

Appendix 1 Notation

A_0	Area enclosed by the centerline of shear flow
A_c	Cross-sectional area bounded by the outer perimeter of the concrete; $A_c = bh$
A_{fl}	Total cross-sectional area of the longitudinal FRP bars
A_{ft}	Cross-sectional area of one transverse FRP (stirrup) bar
b	Width of the beam section
E_c	Elastic modulus of the concrete
E_f, E_s	Elastic modulus of FRP and steel reinforcing bars, respectively
$f_c^{'}$	Cylinder compressive strength of concrete
f_{cr}	Cracking stress of the concrete
f_{fl}, f_{ft}	Smeared (average) FRP stresses in the longitudinal and transverse directions, respectively
f_f	Tensile strength of the FRP
f_{fb}	Strength of the bent region in the FRP bars
h	Height of the beam section
k_{1c}	Ratio of the average compressive stress to the peak compressive stress in the concrete struts, taking into account the tensile stress of concrete
k_{1t}	Ratio of the average tensile stress to the peak tensile stress in the concrete struts
α_2	Fixed angle, angle of applied principal compressive stress (2-axis) with respect to the longitudinal FRP bars (l-axis)
β	Deviation angle
γ_{21}	Smeared (average) biaxial shear strain of concrete in the 2-1 direction
γ_{lt}	Smeared (average) shear strain of FRP bars in the l-t direction
k_{1t}	Ratio of the average tensile stress to the peak tensile stress in the concrete struts
$\bar{\varepsilon}_2, \bar{\varepsilon}_1$	Smeared (average) uniaxial strain of concrete in the 2-direction and the 1-direction, respectively
τ_{21}^{c}	Smeared (average) shear stress of concrete in 2-1 coordinate
τ_{lt}	Applied shear stress in the l-t coordinate of the FRP bars
$\bar{\varepsilon}_{2s}, \bar{\varepsilon}_{1s}$	Maximum uniaxial strain at the surface in the 2-direction and the 1-direction; respectively $\bar{\varepsilon}_{2s} = 2\bar{\varepsilon}_2$ *and* $\bar{\varepsilon}_{1s} = 2\bar{\varepsilon}_1$
ε_{cu}	Maximum strain of concrete
ε_f	FRP bar tensile strain
ε_{fe}	Effective FRP tensile strain
ε_{fu}	Maximum strain of FRP reinforcing bar
$\varepsilon_l, \varepsilon_t$	Smeared (average) biaxial strain of FRP bars in the l-direction and the t-direction, respectively
$\bar{\varepsilon}_l, \bar{\varepsilon}_t$	Smeared (average) uniaxial strain of FRP bars in the l-direction and the t-direction, respectively
ε_{sf}	Smeared (average) strain of steel reinforcing bars that yield first
p_0	Perimeter of centerline of shear flow zone
p_c	Perimeter of outer concrete cross section; $p_c = 2(b+h)$
q	Shear flow
s	Center-to-center spacing of the transverse FRP bars (stirrups)
T	Torque
T_{cr}	Cracking torque
t_d	Effective thickness of shear flow zone
T_u	Ultimate torque
w	Out-of-plane displacement in the direction normal to the membrane element
ε_0	Concrete strain at the peak compressive stress $f_c{'}$ taken as -0.002
$\varepsilon_2, \varepsilon_1$	Smeared (average) biaxial strain of concrete in the 2-direction and the 1-direction, respectively
$\bar{\varepsilon}_l, \bar{\varepsilon}_t$	Smeared (average) uniaxial strain of FRP bars in the l-direction and the t-direction, respectively
ζ	Softening coefficient of concrete in compression

Appendix 1 Notation (continued)

φ	Curvature of the concrete struts along the 1-direction
γ_{21}	Smeared (average) biaxial shear strain of concrete in the 2-1 direction
ρ	FRP reinforcement ratio
ρ_{fl}, ρ_{ft}	Longitudinal and transverse ratios, respectively. $\rho_{fl} = \frac{A_{fl}}{p_0 t_d}$ and $\rho_{ft} = \frac{A_{ft} p_c}{p_0 s t_d}$
v_{12}, v_{21}	Hsu/Zhu ratios used in the SMM
$(v_{12})_{Shear}$	Same as v_{12}
$(v_{12})_{Torsion}$	Modified Hsu/Zhu ratio used in the SMMT for torsion
ψ	Curvature of the concrete struts along the 2-direction
θ	Angle of twist per unit length
θ_{cr}	Cracking angle of twist per unit length
θ_u	Ultimate angle of twist per unit length
σ_2^c, σ_1^c	Smeared (average) normal stresses of concrete in the 2-direction and the 1-direction, respectively
σ_l, σ_t	Applied normal stresses of FRP bars in the l-direction and the t-direction, respectively